

**TRAVELLING-WAVE SIMILARITY SOLUTIONS  
FOR UNSTEADY THIN-FILM FLOWS**

**SITI SABARIAH BINTI ABAS**

**UNIVERSITI SAINS MALAYSIA**

**2016**

**TRAVELLING-WAVE SIMILARITY SOLUTIONS  
FOR UNSTEADY THIN-FILM FLOWS**

by

**SITI SABARIAH BINTI ABAS**

**Thesis submitted in fulfilment of the requirements  
for the degree of  
Doctor of Philosophy**

**December 2016**

## ACKNOWLEDGEMENT

In the Name of Allah, The Most Merciful and The Most Beneficent.

First and foremost, all praises to Allah for giving me the strengths and His Blessing to complete this study. I would like to express my sincere gratitude to my supervisor, Dr. Yazariah Mohd Yatim for her guidance, encouragement and supervision throughout my studies. My sincere thanks to Prof. Stephen Wilson and Dr. Brian Duffy from University of Strathclyde, Glasgow for their invaluable ideas and suggestions in some parts of my research work.

The financial support provided by Ministry Higher Education of Malaysia, Universiti Sultan Zainal Abidin and Universiti Sains Malaysia via an Academic Staff Training Fellowship, Fundamental Research Grant Scheme (Grant No: 203/PMATHS/6711432) and Short Term Research Grant (Grant No: 304/PMATHS/6312095) throughout of the course of my study are gratefully acknowledged.

My deepest gratitude also goes to my parents for their endless love, prayers and supports. Last but not least, my sincere thanks to all my friends and those who have involved directly or indirectly towards the completion of this thesis.

# TABLE OF CONTENTS

Acknowledgement.....	ii
Table of Contents .....	iii
List of Figures .....	vi
List of Symbols.....	x
Abstrak.....	xii
Abstract .....	xiii

## CHAPTER 1 – INTRODUCTION

1.1 Thin-Film Flow .....	1
1.2 Mathematical Modelling of Thin-Film Flows.....	3
1.3 Newtonian and Non-Newtonian Fluids.....	10
1.4 Power-law Model .....	13
1.5 Dry Patches and Rivulets.....	15
1.6 Motivations of Study .....	16
1.7 Problem Statement .....	17
1.8 Aim and Objectives of Study .....	17
1.9 Limitation of Study.....	18
1.10 Research Methodology .....	19
1.11 Shooting Method .....	21
1.12 Thesis Outline .....	22

## CHAPTER 2 – LITERATURE REVIEW

2.1 Thin-Film Fluid Flow Driven by External Forces .....	23
--	----

2.1.1	Steady and unsteady fluid flow of rivulet .....	24
2.1.2	Steady and unsteady fluid flow around dry patch.....	29
2.2	Thin-Film Fluid Flow Driven by Other Forces.....	36
2.3	Conclusion .....	39
<b>CHAPTER 3 – GRAVITY-DRIVEN DRY PATCH IN A NON-NEWTONIAN POWER-LAW FLUID FLOW</b>		
3.1	Problem Specification .....	41
3.2	Numerical Solution.....	53
3.3	Asymptotic Solution.....	55
3.4	Discussion .....	67
<b>CHAPTER 4 – SHEAR-STRESS-DRIVEN DRY PATCH IN A NON-NEWTONIAN POWER-LAW FLUID FLOW</b>		
4.1	Problem Specification .....	68
4.2	Numerical Solution.....	77
4.3	Asymptotic Solution.....	80
4.4	Discussion .....	87
<b>CHAPTER 5 – GRAVITY-DRIVEN DRY PATCH WITH STRONG SURFACE-TENSION EFFECT</b>		
5.1	Problem Specification .....	89
5.2	Numerical Solution.....	101
5.3	Discussion .....	110
<b>CHAPTER 6 – GRAVITY-DRIVEN RIVULET WITH STRONG SURFACE-TENSION EFFECT</b>		
6.1	Problem Specification .....	114

6.2	Numerical Solution.....	121
6.3	Discussion .....	129

**CHAPTER 7 – CONCLUSIONS AND FURTHER WORK**

7.1	Conclusions .....	130
7.2	Suggestions for Future Work.....	133

<b>REFERENCES</b> .....	135
-------------------------	-----

**APPENDICES**

**LIST OF PUBLICATIONS**

## LIST OF FIGURES

		Page
Figure 1.1	Geometry of the two-dimensional thin-film flow down an inclined plane.	8
Figure 1.2	Sketch of simple shearing flow.	11
Figure 1.3	Flow curve for time-independent fluids.	14
Figure 1.4	The breakup of fluid film.	15
Figure 1.5	Flow chart of methodology.	20
Figure 2.1	Example of Duffy and Moffatt's (1997) steady rivulet solution. The inset shows the cross-sectional profile of the rivulet.	27
Figure 2.2	Example of Yatim et al.'s (2011) unsteady single-humped rivulet solution at different times $t$ . The inset shows the cross-sectional profile of the rivulet.	29
Figure 2.3	One-parameter family of solutions parameterised by the velocity of the dry patch for (a) gravity-driven flow (Yatim et al., 2012a) and (b) shear-stress-driven flow (Yatim et al., 2013b).	31
Figure 2.4	Picture of dry patch obtained by Rio et al. (2004).	33
Figure 2.5	Shapes of the dry patch observed by Sébilleau et al. (2015) with an increasing flow rate. The right part of the figure shows the fitted contact line shape with the model of Podgorski et al. (2001) (shown by the white curve), and they are nearly perfect fit.	34
Figure 2.6	A sketch of the unsteady two-dimensional flow studied by Huppert (1982).	36
Figure 2.7	Photos of fluid flowing down an inclined plane at times (a) $t = 0.5$ sec, (b) $t = 4.0$ sec, (c) $t = 8.0$ sec and (d) $t = 84.0$ sec after releases observed by Kondic (2003) where the capillary ridges form just behind the fluid front.	38
Figure 3.1	Geometry of the dry patch in a flowing fluid film driven by gravity.	42

Figure 3.2	Sketch of the predicted dry patch.	49
Figure 3.3	Cross-section of the fluid film.	51
Figure 3.4	Plot of $c$ as a function of $\eta_0$ for (a) $N = 1/20, 1/10, 1/5, 1/2$ and (b) $N = 1$ (as obtained by Yatim et al. (2012a)), 2, 5, 10, 20 shown as the solid lines. The asymptotic value $c = c_\infty = 1$ (3.66) is represented by the dashed line.	56
Figure 3.5	The enlargement of the behavior near $\eta_0 = 0$ for (a) $N = 1/20$ , (b) $N = 1/10$ , (c) $N = 1/5$ , (d) $N = 1/2$ , (e) $N = 1$ (as obtained by Yatim et al. (2012a)), (f) $N = 2$ , (g) $N = 5$ , (h) $N = 10$ and (i) $N = 20$ .	57
Figure 3.6	The cross-section of the fluid profiles $F(\eta)$ for $\eta_0 = 0.5, 2.0$ and $3.5$ when (a) $N = 1/2$ and (b) $N = 2$ .	58
Figure 3.7	The cross-section of the fluid profiles $F(\eta)$ for $N = 1/20, 1/5, 1$ (as obtained by Yatim et al. (2012a)), 5 and 20 when $\eta_0 = 0.1$ .	59
Figure 3.8	Three-dimensional plots when $N = 2$ and $\eta_0 = 0.5$ at (a) $t = 0$ , (b) $t = 1$ and (c) $t = 3$ .	60
Figure 3.9	Three-dimensional plots when $N = 2$ and $t = 1$ at (a) $\eta_0 = 1/2$ , (b) $\eta_0 = 1$ and (c) $\eta_0 = 2$ .	61
Figure 3.10	Numerical solution of (3.51) (shown as the solid line) for $N = 1/2$ when (a) $\eta_0 = 0.0001$ and (b) $\eta_0 = 0.2$ , together with the asymptotic solution of (3.61) (shown as the dashed line) in the limit $\eta_0 \rightarrow 0$ .	63
Figure 3.11	Numerical solution of (3.51) (shown as the solid line) for $N = 1/2$ when (a) $\eta_0 = 0.5$ and (b) $\eta_0 = 5$ , together with the asymptotic solution of (3.67) (shown as the dashed line) in the limit $\eta_0 \rightarrow \infty$ .	65
Figure 3.12	Plot of $q_{\text{area}}$ (3.43) (shown as the solid lines) and $q_{\text{flux}}$ (3.55) (shown as the dot-dashed lines) as a function of $\eta_0$ for $N = 1/5$ and $N = 5$ with the asymptotic solutions in the limit $\eta_0 \rightarrow 0$ (3.71) (shown as the dots) and the asymptotic solution in the limit $\eta_0 \rightarrow \infty$ (3.72) (shown as the dashed lines).	66
Figure 4.1	Geometry of the dry patch in a flowing fluid film driven by shear stress.	69

Figure 4.2	Plot of $c$ as a function of $\eta_0$ . The inset shows an enlargement of the behavior near $\eta_0 = 0$ , where the dots represent $c = c_0 \simeq 1.5424$ , $c = c_{\min} \simeq 1.5421$ and $c = c_{\max} \simeq 1.5503$ . The asymptotic value $c = c_\infty = 1$ (3.66) is represented by the dashed line.	79
Figure 4.3	The cross-section of the fluid profiles $F(\eta)$ for $\eta_0 = 0.1, 1, 3$ and $5$ .	80
Figure 4.4	Three-dimensional plots when $\eta_0 = 0.5$ at (a) $t = 0$ , (b) $t = 1$ and (c) $t = 3$ .	81
Figure 4.5	Three-dimensional plots when $t = 1$ at (a) $\eta_0 = 0.5$ , (b) $\eta_0 = 1$ and (c) $\eta_0 = 1.5$ .	82
Figure 4.6	Numerical solution of (4.39) (shown as the solid line) for (a) $\eta_0 = 0.02$ and (b) $\eta_0 = 0.2$ , together with the asymptotic solution of (4.44) (shown as the dashed line) in the limit $\eta_0 \rightarrow 0$ .	84
Figure 4.7	Numerical solution of (4.39) (shown as the solid line) for (a) $\eta_0 = 1$ and (b) $\eta_0 = 4$ , together with the asymptotic solution of (4.50) (shown as the dashed line) in the limit $\eta_0 \rightarrow \infty$ .	86
Figure 4.8	Plot of $q_{\text{area}}$ (4.34) (shown as the solid line) and $q_{\text{flux}} (= cq_{\text{area}})$ (shown as the dot-dashed line) as a function of $\eta_0$ with the asymptotic solutions in the limit $\eta_0 \rightarrow 0$ (4.51) (shown as the dots) and the asymptotic solution in the limit $\eta_0 \rightarrow \infty$ (4.52) (shown as the dashed line).	87
Figure 5.1	Cross-section of the fluid film with capillary ridge.	95
Figure 5.2	Sketch of the dry patch that travels down the inclined plane in (a) and (c) and travels up the inclined plane in (b) and (d).	101
Figure 5.3	Plot of $c$ as a function of $\eta_0$ for $N = 1/5, 3/10, 2/5, 1/2, 3/5$ and $1$ with $A = -5$ .	104
Figure 5.4	The cross-section of the fluid profiles $F(\eta)$ for $c = 0.3, 0.6, 0.9$ and $1.2$ with $A = -5$ and $N = 1/2$ .	105
Figure 5.5	The cross-section of the fluid profiles $F(\eta)$ for $A = -20, -15, -10, -5$ and $-2$ with $c = 0.5$ and $N = 1/2$ .	105
Figure 5.6	Three-dimensional plots for $S_\ell c < 0, A = -5, c = 1$ when (a) $t = 0$ , (b) $t = 3$ and (c) $t = 6$ with $N = 1$ .	106

Figure 5.7	The cross-section of the fluid profiles $F(\eta)$ for $c = -5, -4, -3, -2$ and $-1$ with $A = -5$ and $N = 1/2$ .	107
Figure 5.8	The cross-section of the fluid profiles $F(\eta)$ for $A = -7, -6, -5, -4$ and $-3$ with $c = -0.3$ and $N = 1/2$ .	108
Figure 5.9	Three-dimensional plots for $S_\ell c < 0, A = -5, c = -1$ when (a) $t = 0$ , (b) $t = 3$ and (c) $t = 6$ with $N = 1$ .	109
Figure 5.10	The cross-section of the fluid profiles $F(\eta)$ for $c = -25, -20, -15, -10$ and $-5$ with $A = -5$ and $N = 2$ .	110
Figure 5.11	The cross-section of the fluid profiles $F(\eta)$ for $A = -25, -20, -15, -10$ and $-5$ with $c = -5$ and $N = 2$ .	111
Figure 5.12	Three-dimensional plots for $S_\ell c > 0, A = -5, c = -1$ when (a) $t = 0$ , (b) $t = 0.5$ and (c) $t = 1$ with $N = 5$ .	112
Figure 6.1	Geometry of the rivulet.	115
Figure 6.2	Plot of $\eta_0$ as a function of $F_0$ for $F_2 = -1, c = 1$ and $N = 1/5, 2/5, 3/5, 4/5$ and $1$ , together with $F_{0c}$ (shown as dots).	123
Figure 6.3	The cross-section of the profiles $F(\eta)$ with $F_0 = 2, 3, 4, 5, 6, 7, 8, 9, F_2 = -1$ and $c = 1$ for (a) $N = 1$ (with $F_{0c} \simeq 1.1990$ ) and (b) $N = 1/5$ (with $F_{0c} \simeq 1.1171$ ).	124
Figure 6.4	The cross-section of the profiles $F(\eta)$ with $F_2 = -4, -3, -2, -1, -0.5, -0.1, -0.01, -0.00001, F_0 = 2, c = 1$ for (a) $N = 1$ and (b) $N = 1/5$ .	125
Figure 6.5	Plot of $I$ and $J$ as function of $F_0$ with $F_2 = -1, c = 1$ for (a) $N = 1$ and (b) $N = 4/5$ .	126
Figure 6.6	Plot of $\eta_0$ as a function of $F_0$ with $F_2 = -1, c = 15$ for $N = 5, 10, 15, 20$ and $100$ .	127
Figure 6.7	Plot of $\eta_0$ as a function of $F_0$ with $F_2 = -1, c = -1$ for $N = 5, 10, 15, 20$ and $100$ .	127
Figure 6.8	Three-dimensional plots for $F_0 = 2, F_2 = -1, c = 1$ at times (a) $t = 1$ , (b) $t = 5$ and (c) $t = 10$ .	128
Figure A.1	Shooting procedure.	146

## LIST OF SYMBOLS

### *Roman letters*

$a$	semi-width of the dry patch/rivulet
$\Delta A$	cross-sectional area difference
$c$	velocity of the dry patch/rivulet
$c_0$	velocity of the dry patch/rivulet at $\eta_0$
$c_\infty$	asymptotic velocity of the dry patch
$c_{\max}$	global maximum velocity of the dry patch/rivulet
$c_{\min}$	local minimum velocity of the dry patch/rivulet
$f$	given function of $\eta$
$F$	functional of $\eta$
$g$	gravitational acceleration
$h$	fluid thickness
$h_\infty$	uniform fluid thickness
$N$	power-law index
$O$	origin in Cartesian coordinate system
$p$	pressure of the fluid
$p_a$	atmospheric pressure
$p_\infty$	uniform fluid pressure
$\Delta Q$	cross-sectional volume difference

$t$	time variable
$u$	fluid velocity in the $x$ -direction
$u_\infty$	uniform fluid velocity in the $x$ -direction
$\bar{u}$	local flux in the $x$ -direction
$U$	depth-averaged velocity
$v$	fluid velocity in the $y$ -direction
$v_\infty$	uniform fluid velocity in the $y$ -direction
$\bar{v}$	local flux in the $y$ -direction
$w$	fluid velocity in the $z$ -direction

*Greek letters*

$\alpha$	angle of the inclination
$\gamma$	shear rate of the fluid
$\eta$	nondimensional similarity variable
$\eta_0$	nondimensional semi-width of the dry patch/rivulet
$\mu$	dynamic viscosity of the fluid
$\mu_0$	consistency coefficient of the fluid
$\rho$	density of the fluid
$\sigma$	surface tension of the fluid
$\tau$	shear stress of the fluid

**PENYELESAIAN KESERUPAAN GELOMBANG MENJALAR BAGI  
ALIRAN FILEM NIPIS TAK MANTAP**

**ABSTRAK**

Kajian aliran filem nipis telah berkembang dengan pesat dalam tahun-tahun kebelakangan ini bagi pelbagai aplikasi, contohnya, aliran lava, dalam proses salutan dan dalam peranti elektronik. Tesis ini bertujuan mengkaji penyelesaian keserupaan gelombang menjalar bagi aliran tak mantap filem nipis tiga dimensi bendalir Newtonan dan bendalir hukum-kuasa bukan Newtonan di atas satah condong. Secara spesifiknya, aliran sekitar tompok kering yang lampai dan aliran bagi jejurus yang lampai dipertimbangkan. Aliran adalah didorong oleh graviti atau tegasan ricih pada permukaan bebas bagi kes kesan tegangan permukaan yang lemah dan kes kesan tegangan permukaan yang kuat. Penghampiran pelinciran diaplikasikan kepada persamaan Navier-Stokes dan persamaan keselanjaran tertakluk kepada syarat sempadan tanpa gelincir dan syarat tiada penembusan, keseimbangan tegasan normal dan tegasan tangen dengan syarat kinematik bagi menghasilkan persamaan pembezaan separa menakluk. Suatu transformasi keserupaan, iaitu penyelesaian keserupaan gelombang menjalar digunakan untuk menurunkan persamaan pembezaan separa menakluk kepada persamaan pembezaan biasa. Persamaan pembezaan tersebut kemudiannya diselesaikan secara berangka dengan kaedah tembakan menggunakan perisian *Mathematica* 9.0. Kajian ini memberikan sumbangan dalam dapatan aliran filem nipis tak mantap bagi bendalir Newtonan dan bendalir hukum-kuasa bukan Newtonan, khususnya bagi aliran sekitar tompok kering yang lampai dan aliran bagi jejurus yang lampai di atas satah condong.

# TRAVELLING-WAVE SIMILARITY SOLUTIONS FOR UNSTEADY THIN-FILM FLOWS

## ABSTRACT

The study of the thin-film flows have developed rapidly in the recent years for various applications, for example, lava flow, in coating process and in electronic devices. This thesis aims to study the travelling-wave similarity solution for unsteady three-dimensional flows of thin films of Newtonian and non-Newtonian power-law fluids on an inclined plane. Specifically, flow around slender dry patch and flow of slender rivulet are considered. The flow is driven by gravity or shear stress at the free surface in the case of weak and strong surface-tension effects. The lubrication approximation is applied to the Navier-Stokes equations and continuity equation subject to the boundary conditions of no slip and no penetration, the balances of normal and tangential stress together with the kinematic condition to yield a governing partial differential equation. A similarity transformation, namely a travelling-wave similarity solution is used to reduce the governing partial differential equation into the ordinary differential equation. The differential equation is then solved numerically using a shooting method via *Mathematica* 9.0 software. This study has provided the significant contribution in the investigation of the unsteady thin-film flow of Newtonian and non-Newtonian power-law fluids, particularly for the flow around the slender dry patch and the flow of slender rivulet on an inclined plane.

# CHAPTER 1

## INTRODUCTION

### 1.1 Thin-Film Flow

The flow of thin-fluid film arises in our daily life, ranging from a very simple process such as rain drop movement down the windowpane to an extreme occurrence such as in lava flows. Appearing in countless practical applications, the field of thin films has attracted many researchers working across a wide range of contexts spanning in the field of biology, industry and geology.

For instance, in biology, thin film appears in lung airways. The serous and mucus layers serve as a protective coating to prevent the drying of the underlying cells and a trap to the inhaled pathogens (Grotberg, 1994, 2001). Thin film also appears in the tear film in human eyes. The tear film that builds up in a few microns thick is being distributed through the eyes by blinking. This is critical for good vision, provides an optically smooth surface for light refraction, keeps the cornea surface moist and protects the eye with bactericidal enzymes. Rupture or insufficient of tear film may lead to severe damage to the corneal surface such as eye irritation and corneal ulceration. For a contact lens wearer, the sufficient pre-lens tear film (between the cornea and the contact lens) and post-lens tear film (between the contact lens and the outside environment) are crucial in oxygen transport to the cornea (Wong et al., 1996).

In industry, thin film is used in coating process, a process by which one or more thin layers of liquid are applied to a surface. It is either for protection, decoration or

information storage. They find uses in various applications such as in adhesives, beverage containers, magnetic tapes, photographic films, microelectronics fabrications and on surfaces of compact disk roms. It is of prime importance to make sure the coating layer is uniform, thin, highly accurate and defect-free. Air entrainments, contaminants and excessive acceleration of application, causing a non-continuous layer and ruptures of thin film, must be avoided to produce a high quality end product (Ruschak, 1985; Dandapat et al., 2003; Daripa and Paşa, 2009). Familiar applications of thin film also arise in paint levelling industry (Figliuzzi et al., 2012), coating paper industry (Kaulakis, 1974) and in heat and transfer process, such as in refrigerator, condenser, cooling devices and in heat exchanger design (Focke and Knibbe, 1986; Vlasogiannis et al., 2002).

In geology, applications of thin film arise in numerous occurrences of gravity currents, which take place whenever a fluid flows horizontally into another fluid due to the density difference (Huppert and Simpson, 1980; Federico et al., 2006; Huppert, 2006). Examples of that occurrences are thunderstorm outflows, propagations of sea-breeze fronts, estuaries, flows of industrial waste into the rivers, oil spreadings on the sea (Hoult, 1972) as well as lava flows (Balmforth et al., 2000; Griffiths, 2000). Other geophysical examples also include snow avalanches (Ancy, 2007) and ice sheet models (Baral et al., 2001).

There are also a considerable mathematical interests in dealing with the analysis of thin-film equations themselves as discussed by Myers (1998) who reviewed the thin-fluid film for which the surface tension is a driving mechanism, King (2001) on derivation of thin-film equation, Becker and Grün (2005) who discussed the analyt-

ical achievements for various types of thin-film equation and Qu (2006) who studied the symmetry solution to the thin-film equation. Other works includes Momoniat (2011) who studied the thin-film equation associated with boundary value problems numerically, and Charalambous and Sophocleous (2013) who studied the symmetry properties of a generalized thin-film equation. Recently, Al Mukahal et al. (2015a,b) studied the thin-film equation associated with the contact angle, Peng et al. (2016) studied the thin-film equation with a diffusion term, Giacomelli et al. (2016) obtained the travelling-wave solutions of the thin-film equation with zero microscopic contact angle and inhomogeneous mobility, and Qu and Zhou (2016) studied the initial-value problem of the thin-film equation with the nonlocal source in a bounded domain. It is important to note that, almost all the mentioned works regarding the thin-fluid film are derived from the thin-film lubrication theory.

## 1.2 Mathematical Modelling of Thin-Film Flows

In general, the mathematical model of incompressible fluid flow is provided by the Navier-Stokes equations, named after Claude-Louis Navier and George Gabriel Stokes. It can be viewed as an application of Newton's second law together with the fluid stress.

Consider

$$\rho \frac{D\mathbf{u}}{Dt} = \rho \mathbf{f} + \nabla \cdot \mathbf{T}, \quad (1.1)$$

with the incompressibility condition

$$\nabla \cdot \mathbf{u} = 0, \quad (1.2)$$

where  $\rho$  is the density,  $\mathbf{u}$  is the fluid velocity,  $t$  is the time,  $\mathbf{f}$  is the body force,  $\nabla$  is the usual vector differential gradient operator,  $\frac{D}{Dt} = \frac{\partial}{\partial t} + \mathbf{u} \cdot \nabla$  is the usual convective derivative and  $\mathbf{T}$  is the stress tensor. For the Newtonian fluid, the stress tensor is the linear function of the shear rate (to be discussed further in Section 1.3) given by

$$\mathbf{T} = -p\mathbf{I} + \mu \left[ \nabla \mathbf{u} + (\nabla \mathbf{u})^T \right], \quad (1.3)$$

where  $p$  is the fluid pressure,  $\mathbf{I}$  is the identity tensor and  $\mu$  is the fluid viscosity.

If the flow is two-dimensional in the  $x$ - $y$  plane, (1.2) takes the form of

$$\frac{\partial u}{\partial x} + \frac{\partial v}{\partial y} = 0, \quad (1.4)$$

and the generalization of (1.3) takes the form of

$$\mathbf{T} = \begin{pmatrix} -p + 2\mu \frac{\partial u}{\partial x} & \mu \left( \frac{\partial u}{\partial y} + \frac{\partial v}{\partial x} \right) \\ \mu \left( \frac{\partial u}{\partial y} + \frac{\partial v}{\partial x} \right) & -p + 2\mu \frac{\partial v}{\partial y} \end{pmatrix}. \quad (1.5)$$

A straightforward substitution of (1.5) into (1.1) yields

$$\rho \left( \frac{\partial u}{\partial t} + u \frac{\partial u}{\partial x} + v \frac{\partial u}{\partial y} \right) = \rho f_x - \frac{\partial p}{\partial x} + \mu \left( \frac{\partial^2 u}{\partial x^2} + \frac{\partial^2 u}{\partial y^2} \right), \quad (1.6)$$

in the  $x$ -direction, and

$$\rho \left( \frac{\partial v}{\partial t} + u \frac{\partial v}{\partial x} + v \frac{\partial v}{\partial y} \right) = \rho f_y - \frac{\partial p}{\partial y} + \mu \left( \frac{\partial^2 v}{\partial x^2} + \frac{\partial^2 v}{\partial y^2} \right), \quad (1.7)$$

in the  $y$ -direction or, (1.6) and (1.7) can be written more compactly in the vector form

$$\rho \frac{D\mathbf{u}}{Dt} = \rho \mathbf{f} - \nabla p + \mu \nabla^2 \mathbf{u}. \quad (1.8)$$

Equation (1.8) is called the Navier-Stokes equation for incompressible Newtonian fluid (Batchelor, 1967). For the non-Newtonian power-law fluid, the stress tensor however is a nonlinear function of the shear rate, to be discussed in Section 1.3. In order to solve (1.2) and (1.8), the appropriate boundary conditions need to be applied. Three types of boundary conditions must be considered which are the cases when the fluid is in contact with a solid (fluid-solid boundary), when the fluid is in contact with another fluid (fluid-fluid boundary) and when the fluid is unbounded (Subramanian and Balasubramaniam, 2001; Shankar, 2007).

At fluid-solid boundary, the tangential component of velocity satisfies the no slip condition:

$$\mathbf{u} \cdot \mathbf{t} - \mathbf{U} \cdot \mathbf{t} = 0, \quad (1.9)$$

while the normal component of velocity satisfies the no penetration condition:

$$\mathbf{u} \cdot \mathbf{n} - \mathbf{U} \cdot \mathbf{n} = 0, \quad (1.10)$$

where  $\mathbf{U}$  is the velocity of the solid,  $\mathbf{t}$  is a unit vector tangent to the boundary and  $\mathbf{n}$  is the unit vector normal to the boundary. Combining (1.9) and (1.10) yields

$$\mathbf{u} = \mathbf{U}, \quad (1.11)$$

which means that the velocity of the fluid is equal to the velocity of solid boundary.

However, if the boundary is stationary,

$$\mathbf{u} = \mathbf{0}. \quad (1.12)$$

Note that it is also possible to incorporate the slip condition but it is not considered here (Richardson, 1989; Paterson, 2013).

At fluid-fluid boundary, the stress balance equation is given by

$$\mathbf{n} \cdot \mathbf{T} - \mathbf{n} \cdot \bar{\mathbf{T}} = \sigma \mathbf{n} (\nabla \cdot \mathbf{n}) - \nabla \sigma, \quad (1.13)$$

where  $\mathbf{T}$  is the stress tensor in the first fluid,  $\bar{\mathbf{T}}$  is the stress tensor in the second fluid and  $\sigma$  is the surface tension between the fluids. In the case of free-surface flow, (1.13) reduces to

$$\mathbf{n} \cdot \mathbf{T} = \sigma \mathbf{n} (\nabla \cdot \mathbf{n}) - \nabla \sigma \quad (1.14)$$

and if the surface tension is constant (which is often considered to be), the balances of normal stress obtained by multiplying both sides of (1.14) by  $\mathbf{n}$  is given by

$$\mathbf{n} \cdot \mathbf{T} \cdot \mathbf{n} = \sigma (\nabla \cdot \mathbf{n}), \quad (1.15)$$

and the tangential stress obtained by multiplying both sides of (1.14) by  $\mathbf{t}$  is given by

$$\mathbf{n} \cdot \mathbf{T} \cdot \mathbf{t} = 0. \quad (1.16)$$

In addition, the kinematic boundary condition,

$$\frac{Df}{Dt} = 0, \quad (1.17)$$

is complemented at the free surface where  $f$  is the equation for the boundary. In the situation where the fluid is unbounded, it is assumed that the uniform condition is held at the far field (Richardson, 1989; Pozrikidis, 2009; Leslie, 2012; Paterson, 2013).

Equations (1.2) and (1.8), in general, have to be solved numerically. However, when the film is thin, these equations can be greatly simplified via the lubrication approximation based on relative smallness of the ratio,

$$\delta = \frac{H}{L} \ll 1, \quad (1.18)$$

where  $H$  and  $L$  are the typical thickness and length, respectively (the value of  $\delta$  may extends from a few micrometre to nanometre (Acheson, 2005; Andras, 2005)), in which the flow is predominantly in the direction of the longer length scale. This simplification may be illustrated by considering a basic example of gravity-driven two-dimensional thin-film flow on an inclined plane as shown in Figure 1.1.

Consider a two-dimensional thin film of Newtonian fluid flows down a stationary plane inclined at angle  $\alpha$  to the horizontal with constant density  $\rho$  and viscosity  $\mu$ . Using Cartesian coordinates  $Oxy$ , the  $x$ -axis is in the direction of the flow and  $y$ -axis is normal to the substrate. The substrate is at  $y = 0$  while the free surface of the fluid is at  $y = h$ , where  $h = h(x, t)$  is the fluid thickness. The problem is re-scaled and

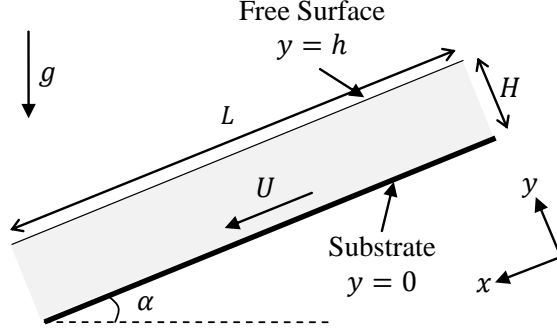


Figure 1.1: Geometry of the two-dimensional thin-film flow down an inclined plane.

non-dimensionalised by writing

$$\begin{aligned}
 x &= Lx^*, & y &= Hy^*, & h &= Hh^*, & t &= \frac{L}{U}t^*, \\
 u &= Uu^*, & v &= \frac{UH}{L}v^*, & p - p_a &= \frac{\mu U}{\delta^2 L}p^*, & \mathbf{T} &= \frac{\mu U}{L}\mathbf{T}^*,
 \end{aligned}
 \tag{1.19}$$

where  $u$  and  $v$  are the components of velocity in the  $x$ - and  $y$ -directions, respectively,  $U = \delta^2 L^2 \rho g / \mu$  is a characteristic velocity in the  $x$ -direction,  $p_a$  is the atmospheric pressure and  $g$  is the gravitational acceleration. With the asterisk dropped for clarity, equations (1.4), (1.6) and (1.7) become

$$\frac{\partial u}{\partial x} + \frac{\partial v}{\partial y} = 0, \tag{1.20}$$

$$\delta^2 Re \left( \frac{\partial u}{\partial t} + u \frac{\partial u}{\partial x} + v \frac{\partial u}{\partial y} \right) = -\frac{\partial p}{\partial x} + \delta^2 \frac{\partial^2 u}{\partial x^2} + \frac{\partial^2 u}{\partial y^2} + \sin \alpha, \tag{1.21}$$

$$\delta^4 Re \left( \frac{\partial v}{\partial t} + u \frac{\partial v}{\partial x} + v \frac{\partial v}{\partial y} \right) = -\frac{\partial p}{\partial y} + \delta^2 \left( \delta^2 \frac{\partial^2 v}{\partial x^2} + \frac{\partial^2 v}{\partial y^2} \right) - \delta \cos \alpha, \tag{1.22}$$

where  $Re = \rho UL / \mu$  is the well-known Reynolds number. At leading order in the thin-film limit  $\delta \rightarrow 0$ , equations (1.20)-(1.22) simplify to

$$\frac{\partial u}{\partial x} + \frac{\partial v}{\partial y} = 0, \tag{1.23}$$

$$0 = -\frac{\partial p}{\partial x} + \frac{\partial^2 u}{\partial y^2} + \sin \alpha, \quad (1.24)$$

$$0 = -\frac{\partial p}{\partial y}, \quad (1.25)$$

respectively. The equations (1.23)-(1.25) are often referred to as the lubrication equations which has been obtained based on the assumptions that  $\delta \ll 1$  and the reduced Reynolds number  $\delta^2 Re = \delta^2 \rho UL / \mu$  are small; in particular, this means that  $Re$  itself need not be small. At the stationary inclined plane  $y = 0$ , the conditions of no slip and no penetration given by (1.12), respectively, are simply

$$u = v = 0. \quad (1.26)$$

At the free surface  $y = h(x, t)$ , the kinematic condition  $D(h - y) / Dt = 0$  from (1.17), is given by

$$\frac{\partial h}{\partial t} + u \frac{\partial h}{\partial x} - v = 0 \quad (1.27)$$

and the stress balance equations are given by (1.15) and (1.16) where the stress tensor is

$$\mathbf{T} = \begin{pmatrix} -\frac{\mu U}{\delta^2 L} p + \frac{2\mu U}{L} \frac{\partial u}{\partial x} & \frac{\mu U}{H} \frac{\partial u}{\partial y} + \frac{\mu U \delta}{L} \frac{\partial v}{\partial x} \\ \frac{\mu U}{H} \frac{\partial u}{\partial y} + \frac{\mu U \delta}{L} \frac{\partial v}{\partial x} & -\frac{\mu U}{\delta^2 L} p + \frac{2\mu U}{L} \frac{\partial v}{\partial y} \end{pmatrix} \quad (1.28)$$

and the unit normal vector and the unit tangent vector are

$$\mathbf{n} = \frac{\left(-\delta \frac{\partial h}{\partial x}, 1\right)}{\left[1 + \delta^2 \left(\frac{\partial h}{\partial x}\right)^2\right]^{\frac{1}{2}}}, \quad \mathbf{t} = \frac{\left(1, \delta \frac{\partial h}{\partial x}\right)}{\left[1 + \delta^2 \left(\frac{\partial h}{\partial x}\right)^2\right]^{\frac{1}{2}}}, \quad (1.29)$$

respectively, with

$$\nabla \cdot \mathbf{n} = -\frac{\frac{\delta}{L} \frac{\partial^2 h}{\partial x^2}}{\left[1 + \delta^2 \left(\frac{\partial h}{\partial x}\right)^2\right]^{\frac{3}{2}}}. \quad (1.30)$$

Therefore from (1.15) and (1.16), the full boundary conditions at the free surface are

$$\frac{1}{1 + \left(\delta \frac{\partial h}{\partial x}\right)^2} \left[ \delta^2 \left( 2 \frac{\partial u}{\partial x} \left( \frac{\partial h}{\partial x} \right)^2 - 2 \frac{\partial v}{\partial x} \frac{\partial h}{\partial x} \right) - \frac{p}{\delta^2} - \left( \frac{\partial h}{\partial x} \right)^2 p - \right. \\ \left. 2 \frac{\partial u}{\partial y} \frac{\partial h}{\partial x} + 2 \frac{\partial v}{\partial y} \right] \frac{\mu U}{L} = - \frac{\sigma \delta \frac{\partial^2 h}{\partial x^2}}{L \left[ 1 + \left( \delta \frac{\partial h}{\partial x} \right)^2 \right]^{\frac{3}{2}}}, \quad (1.31)$$

and

$$\frac{1}{1 + \left(\delta \frac{\partial h}{\partial x}\right)^2} \left[ \frac{\partial u}{\partial y} + \delta \left( \frac{\partial v}{\partial x} - 2 \frac{\partial u}{\partial x} \frac{\partial h}{\partial x} + 2 \frac{\partial v}{\partial y} \frac{\partial h}{\partial x} - \frac{\partial u}{\partial y} \left( \frac{\partial h}{\partial x} \right)^2 \right) - \right. \\ \left. \frac{\partial v}{\partial x} \left( \frac{\partial h}{\partial x} \right)^2 \delta^3 \right] \frac{\mu U}{L} = 0, \quad (1.32)$$

respectively. At the leading order in the thin-film limit  $\delta \rightarrow 0$ , (1.31) and (1.32) simplify into

$$-p = -C^{-1} \frac{\partial^2 h}{\partial x^2}, \quad (1.33)$$

$$\frac{\partial u}{\partial y} = 0, \quad (1.34)$$

where  $C = \mu U / \sigma \delta^3$  is the capillary number and it is considered that  $C = O(1)$  (that is,  $\delta = O(\mu U / \sigma)^{1/3}$ ) so that the terms balance in (1.33) (Paterson, 2013). It is worth mentioning that the notations used in this chapter is limited to the example described in this chapter.

### 1.3 Newtonian and Non-Newtonian Fluids

The fluid can be broadly classified as the Newtonian and non-Newtonian fluids, depending on the relationship between the shear stress and the shear rate. This may be explained by referring to the steady simple shearing flow for a fluid confined between

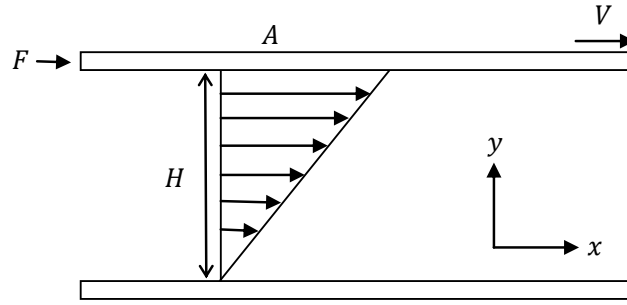


Figure 1.2: Sketch of simple shearing flow.

two parallel plates of area  $A$  separated by a distance  $H$  apart as shown in Figure 1.2. The lower plate is stationary and the upper plate is moving with velocity  $V$  due to a shearing force  $F$ . The ratio of the force to the surface area is the shear stress, denoted as  $\tau$  ( $\tau = F/A$ ), while the ratio of the difference in velocity between the plates to the distance that separated them is the shear rate, denoted as  $\gamma$  ( $\gamma = V/H$ ). According to Newton's law of viscosity, the relationship between the shear stress and the shear rate of the fluid is given by

$$\tau = \mu\gamma, \quad (1.35)$$

where  $\mu$  is a viscosity constant which measure the fluid's resistance to flow.

A Newtonian fluid, named after Sir Isaac Newton, is a fluid that has a linear relationship between the shear stress and the shear rate; or the fluid viscosity is independent of the shear rate. Water and gases are examples of the Newtonian fluid.

In contrast to the Newtonian fluid, a non-Newtonian fluid is a fluid that has a non-linear relationship between the shear stress and the shear rate; or the fluid viscosity depends on the shear rate. There are many types of non-Newtonian fluids which can be categorized into time-independent fluid (pseudoplastic, dilatant and viscoplastic fluids), time-dependent fluid (thixotropic and rheopectic fluids) and viscoelastic fluid.

Each of these types of fluid has its distinct behaviors.

The time-independent fluid is a fluid for which the shear rate at any point is determined only by the shear stress at that point and depends on nothing else. The pseudo-plastic fluid or also known as a shear-thinning fluid is characterized when the viscosity of the fluid decreases with increasing of shear rate. The famous example of this type of fluid is ketchup. One might get a very minimal flow when the ketchup bottle is just turned upside down. Alternatively, a vigorous shake to the bottle will increase the shear rate which results in the decreasing of the ketchup's viscosity, and therefore allows the ketchup to flow more easily.

The dilatant fluid or also known as a shear-thickening fluid on the other hand is characterized when the viscosity of the fluid increases with increasing of shear rate. A mixture of cornflour and water exhibits this property. Stirring the mixture will increase the shear rate which results in the increasing of the mixture's viscosity. Hence, the mixture becomes thicker and difficult to stir. As soon as the mixture is left unstirred, the mixture becomes runny again.

The viscoplastic fluid is characterized by the existence of the yield stress  $\tau_0$ ; a stress that must be exceeded in order for the fluid begin to deform or flow which is given by

$$\tau = \tau_0 + \mu\gamma, \quad \tau > \tau_0. \quad (1.36)$$

Below the yield stress ( $\tau < \tau_0$ ) the viscoplastic fluid will behave like a solid. Basically, there are two types of viscoplastic fluid; one is Bingham plastic in which the flow curve of shear stress against shear rate is linear and another is yield-pseudoplastic in

which the flow curve of shear stress against shear rate is non linear. Toothpaste is one of the common example that display viscoplastic characteristic. It will not flow until an adequate force is applied to the tube. The flow curve for time-independent fluid is shown in Figure 1.3.

Opposite to the time-independent fluids explained above, the viscosity of time-dependent fluids depend not only on the shear rate, but also on the amount of time for which the fluid have been subjected to shearing. The viscosity of thixotropic fluid will decrease with time at a constant shear rate. Examples of materials exhibiting this behavior are cement paste and mud suspensions. On the contrary, the viscosity of the rheopectic fluid will increase with time at a constant shear rate. Examples of materials exhibiting this behavior include coal-water slurries and protein solution. The fluid which possesses both solids (elastic) and fluids (viscous), is referred to as a viscoelastic fluid. Polymer melts and soap solutions are some of the materials that exhibit this behavior (Wilkinson, 1960; Chhabra and Richardson, 2008). Our study will be concerned only with Newtonian, pseudoplastic and dilatant fluids.

#### **1.4 Power-law Model**

There are many rheological formula of varying complexity and forms that had been proposed in the literature to describe the feature of non-Newtonian behavior. Some of them are power-law model, Carreau viscosity equation, Cross viscosity equation, Ellis fluid model, Bingham plastic model, Herschel-Bulkley fluid model and Casson fluid model.

Amongst of these models, power-law model offers the simplest two-parameter

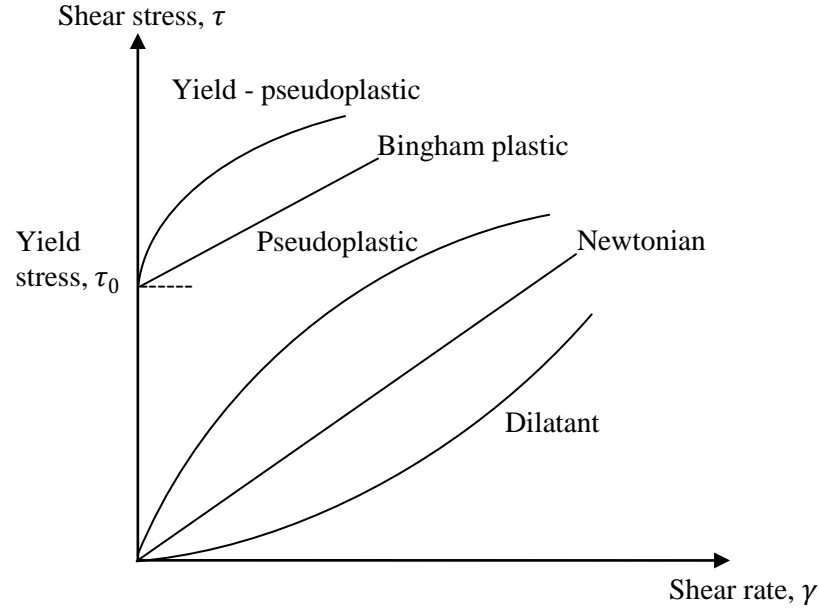


Figure 1.3: Flow curve for time-independent fluids.

model and is widely used in the literature. This model was originally proposed by Ostwald and de Waele, represented by

$$\tau = K\gamma^N. \quad (1.37)$$

By combining (1.35) and (1.37), the viscosity for the power-law fluid is

$$\mu = K\gamma^{N-1}, \quad (1.38)$$

where  $K$  is the fluid consistency coefficient; the higher the value of  $K$  the more viscous the fluid, and  $N$  is the power-law index; greater departures from unity showing more pronounced non-Newtonian properties of the fluid. It is used to describe shear-thinning behavior when  $N < 1$  and shear-thickening behavior when  $N > 1$ . When  $N = 1$ , (1.38) reduces to Newtonian model. However, the power-law model has some drawbacks. Generally, it applies over only a narrow interval of shear rates, lack of ability to de-

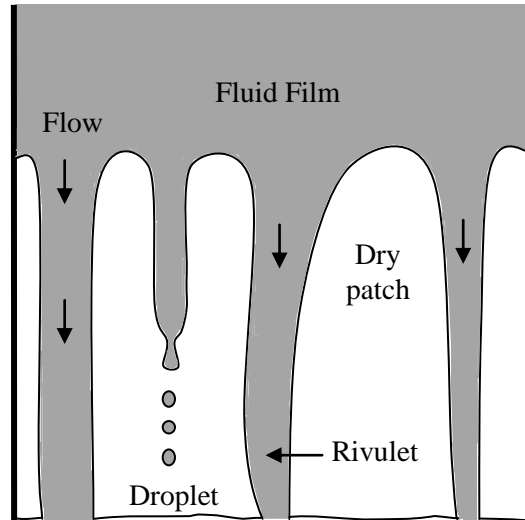


Figure 1.4: The breakup of fluid film.

scribe zero-shear viscosity and infinite-shear viscosity and the dimension of  $K$  depends on the value of  $N$  and therefore the values of  $K$  must not be compared when the values of  $N$  are different. In engineering application, these drawbacks however are not serious (Wilkinson, 1960; Harris, 1977; Chhabra and Richardson, 2008).

### 1.5 Dry Patches and Rivulets

During the draining of the fluid film on an inclined plane or a vertical plane, one may identify the formation of rivulets, droplets or growing dry patches, as shown in Figure 1.4. The dry patch is a non-wettable surface while the narrow stream between them is called a rivulet. Dry patch may occur in a fluid film for a variety of reasons. The formation can be caused by the film rupture; due to the evaporation (Kheshgi and Scriven, 1991), the fluid dry-out which causes critical heat flux (Sharon and Orell, 1980; Anglart, 2015), the film being too thin (Silvi and Dussan, 1985), the surface being partially wetted (Taylor and Michael, 1973; Sharma and Ruckenstein, 1989) and the presence of surface contaminations (Marshall and Wang, 2005). The inhomogeneities between the substrate, air trapped within the film, uneven heating and wave

motion may also initiate the dry patch.

## **1.6 Motivations of Study**

There are two major motivations in this study. The first one is the work by Yaitim et al. (2013a) who studied the unsteady thin film of Newtonian fluid flow that travels around a slender dry patch down an inclined plane. This work considered the travelling-wave similarity solution for the flow driven by gravity and/or a prescribed constant shear stress on the free surface of the film, where the surface tension effect is considered negligible. This study concluded that for both driving mechanisms, the dry patch has a parabolic shape which may be concave up or concave down the substrate and the film thickness is found to increase monotonically away from the contact lines to its uniform far-field value. The second one is the work by Wilson et al. (2001) who studied the steady thin film of Newtonian fluid flow that travels around a slender dry patch under gravity down an inclined plane. The similarity solutions are obtained both for the case of weak and strong surface-tension effects. For the case of weak surface-tension effect, the solution predicts that the dry patch has a parabolic shape and the transverse profile of the free surface has a monotonically increasing shape far from the contact line. For the case of strong surface-tension effect, the solution predicts that the dry patch has a quartic shape and the transverse profile of the free surface has a capillary ridge near the contact line which decays in an oscillatory manner far from it.

Therefore, motivated by these works, we would like to extend the work in finding the travelling-wave similarity solution of the unsteady non-Newtonian power-law fluid around a dry patch, both for gravity-driven flow and shear-stress-driven flow. Since

consideration of surface-tension effect influences the steady flow of Newtonian fluid, it is interesting to figure out whether the presence of that strong surface-tension effect gives similar observation to the unsteady Newtonian fluid and non-Newtonian fluid that flow around a dry patch as well as to the rivulet flow.

### **1.7 Problem Statement**

Over the past few years, a number of studies had been successfully showed the similarity solution for the various thin film encountered in steady and unsteady fluid flows either for weak or strong surface-tension effect. Travelling-wave similarity solution is one of the important class of solution that represents the shape of the wave that travels with the specific speed. In mathematical physics, this type of solution plays an important role because it provides the distribution of the properties of the motion at different times (Barenblatt, 1996; Scott, 2006). Hence, the travelling-wave similarity solution have been carefully studied (see for example; Perazzo and Gratton (2003, 2004) and Pritchard et al. (2015)). However, the study of travelling-wave similarity solution for unsteady three-dimensional flow around a dry patch and flow of rivulet is still lacking and this is a gap that need to be dealt with. Therefore, this study will attempt to address this gap. This study will contribute to a new knowledge in understanding and illustrating the fluid flows considered in the thesis.

### **1.8 Aim and Objectives of Study**

The aim of this thesis is to analyse the travelling-wave similarity solution for unsteady three-dimensional thin-film flow around a slender dry patch and the flow of a slender rivulet on an inclined plane, for both gravity-driven and surface shear-stress-

driven flows in the cases of weak and strong surface-tension effects. The Newtonian and non-Newtonian power-law fluids shall be considered. Therefore, the objectives pursued in this thesis are:

1. to construct mathematical model by using the Navier-Stokes and continuity equations based on the lubrication theory,
2. to carry out the mathematical formulations and analyses which involve the appropriate boundary conditions,
3. to seek the travelling-wave similarity solution of the appropriate governing equations and
4. to obtain the numerical solutions of the ordinary differential equations for thin film by using the shooting method.

In particular, this thesis focuses on four main problems which are gravity-driven dry patch in a non-Newtonian power-law fluid flow, shear-stress-driven dry patch in a non-Newtonian power-law fluid flow, gravity-driven dry patch with strong surface-tension effect and gravity-driven rivulet with strong surface-tension effect.

### **1.9 Limitation of Study**

This study is limited to problems involving unsteady, three-dimensional thin-film flow of Newtonian and non-Newtonian power-law fluids on an inclined plane which are formulated using travelling-wave similarity solution and solved using shooting method. Besides, this study relies on the numerical results and simulations since there

is no theoretical or experimental work is conducted. The solutions showed in this study are also limited to a certain value of power-law index of non-Newtonian fluid.

## 1.10 Research Methodology

The methodology approaches undertaken in this study are the following:

### 1. Problem Formulation

The thin-film lubrication theory within the framework of Navier-Stokes and continuity equations are derived. The mathematical model of each problem highlighted in Section 1.8 is constructed. Particularly, the unsteady three-dimensional thin-film flow down an inclined plane is modelled.

### 2. Similarity Transformation and Non-dimensionalisation

A similarity transformation, namely a travelling-wave similarity solution is employed and the governing partial differential equation is transformed into the ordinary differential equation. The ordinary differential equation is non-dimensionalised to reduce the number of parameters.

### 3. Numerical Computation

The ordinary differential equation with the appropriate boundary conditions is treated as an initial value problem. It is solved by using shooting method via *Mathematica* 9.0 software with `NDSolve` built-in function.

The workflow is presented in Figure 1.5.

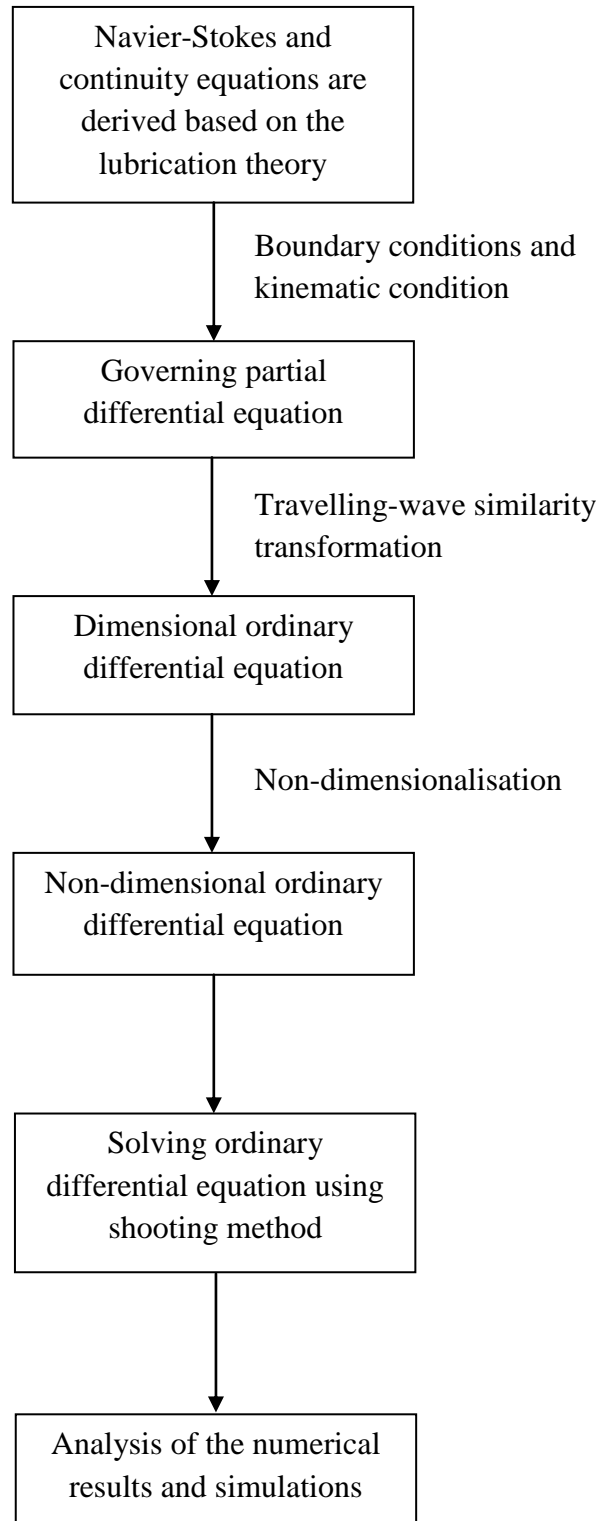


Figure 1.5: Flow chart of methodology.

## 1.11 Shooting Method

In this thesis, the system of nonlinear ordinary differential equation that governs the thin-film flow is the system of two-point boundary value problem. There are variety of numerical methods have been designed to solve two-point boundary value problem including interpolation method, variational method, collocation method, finite difference method and shooting method. However, shooting method is known as a straightforward method, requires minimum problem analysis and preparation, applicable to a wide variety of differential equation and provides a better accuracy (Roberts and Shipman, 1972; Keller, 1976; Hoffman and Frankel, 2001; King and Mody, 2010).

The idea of shooting method is to "shoot" from an initial point to a desired solution at the terminal point by applying the technique designed for the initial value problem. For the nonlinear differential equation, the shooting process is iterative where a sequence of initial values is generated with the hope that it satisfies the given terminal point conditions. The shooting scheme essentially works as follows; by using trial and error (for a small system or simple boundary conditions) or some scientific approach, any unspecified initial value is guessed. The differential equation is then integrated numerically as an initial value problem to the terminal point. The values obtained at the terminal point are compared with the actual boundary condition supplied. If a difference exists, another initial value is guessed and the system of ordinary differential equation is solved again. This process is continued until the terminal point conditions are satisfied to some degree of accuracy (Meyer, 1973; Na, 1979; Asaithambi, 1995; King and Mody, 2010; Faires and Burden, 2012). The example of shooting algorithm for nonlinear second-order boundary value problem is given in Appendix A.

There is a vast literature on shooting methods in solving the thin-film flow problems. Examples are Eres et al. (2000), Myers et al. (2004), Ajaev (2005) and Yatim et al. (2010, 2011, 2012a,b, 2013a,b). In this thesis, all problems have been solved via the shooting technique with *Mathematica*'s `NDSolve`; a function that by default uses an Adams and a backward differentiation formula (BDF) methods (Kallaher, 1999).

## 1.12 Thesis Outline

This thesis is divided into seven chapters. The introduction of the research which consists of the introduction of thin-film flow, the mathematical modelling of thin-film flow, the types of fluid, the motivations of study, the problem statement, the aim and objectives of study, the limitation of study and the research methodology are given in Chapter 1. The related literatures are covered in Chapter 2. Then, all the four problems considered will be discussed in Chapter 3 to Chapter 6. The unsteady flow of thin-fluid film around a slender dry patch on an inclined plane for the flow driven by gravity is presented in Chapter 3 and for the flow driven by surface shear stress is presented in Chapter 4. The fluid is non-Newtonian and the surface tension is considered negligible. The numerical and asymptotic solutions are obtained for each problem. In Chapter 5, the unsteady flow of thin-fluid film around a slender dry patch on an inclined plane for the flow driven by gravity when the surface tension is not negligible is studied. Both Newtonian and non-Newtonian fluids are considered. In Chapter 6, a different type of flow is considered, namely a gravity-driven rivulet flow. The numerical solution is implemented for both problems. Finally, conclusions of the research and recommendations on possible future work are made in Chapter 7.

## CHAPTER 2

### LITERATURE REVIEW

The study of thin-film fluid flow has received a great attention amongst the researchers in recent years. One of the oldest and remarkable study of thin-film flow dates back to 1898 by Hele-Shaw, who investigated the flow in a Hele-Shaw cell. In general, it is the flow of a fluid between two parallel flat plates which are separated by a small gap (Batchelor, 1967; Acheson, 2005). The driving force for the flow can include either of external forces such as gravity, shear force, frictional force and rotating substrate, or of other potential forces such as surface tension and capillary effects.

In this chapter, the relevant literatures related to thin-film fluid flow are outlined. Some key ideas to our study are also highlighted. We start by reviewing the literatures on the thin fluid that flows under the influence of external forces in Section 2.1. Our further study in regards to gravity-driven flow is presented in Chapter 3, Chapter 5 and Chapter 6, and in regards to shear-stress-driven flow is presented in Chapter 4. Next in Section 2.2, the literatures on thin fluid in which the flow is governed by the other forces are briefly discussed. Our current study considering the surface-tension effect is addressed in Chapter 5 and Chapter 6.

#### **2.1 Thin-Film Fluid Flow Driven by External Forces**

The flow of the fluid can be classified into two categories; steady and unsteady flows. It may break up, forming several forms namely fingers (rivulets), dry patches

or droplets. The familiar natural phenomenon of thin-film flow is the motion of rain running down a window pane or on an inclined roadway under the action of gravity. Rivulets of rain with the dry patches in between and drops of rain may developed. Particularly in industry for example, the thin-film flow is used to increase the heat and mass transfer rates and the efficiency operation of many equipments, such as in evaporators and reactors. The breakdown of the fluid is always undesirable in the process since it may reduce the efficiency and may effect the quality of the end products. In this case, understanding the behavior of the flow becomes essential to design such industrial equipments which at least can help in preventing the breakdown of the fluid. Since the thin-film theories have been applied in a wide range of problems, many works have been devoted on both steady and unsteady flows problems.

### **2.1.1 Steady and unsteady fluid flow of rivulet**

The subject of steady thin-film fluid flow had been considered previously by many authors. Astarita et al. (1964) studied the steady flow of non-Newtonian fluid on an inclined plane at low shear stress while Perazzo and Gratton (2003, 2004) studied the steady flow of non-Newtonian power-law fluid on an inclined plane under the action of gravity and viscous stress. The three families of travelling-wave solutions are observed, which are downslope travelling-wave with a front, downslope travelling-wave without front and upslope travelling-wave. The modification on governing equation to include surface-tension effect was proposed by Perazzo and Gratton (2003) and was found to be more relevant when the curvature of the free surface is large, which occurs near to the front. The general formula for the travelling-wave was derived by Perazzo and Gratton (2004) that can be of several kinds according to the value of the propaga-